Sensors and Materials, Vol. 36, No. 1 (2024) 269–276
MYU Tokyo

S & M 3517

Characterization of Plasma-etched Surfaces of TlBr Crystals for Radiation Detectors

Taro Nojima,[1,3*] Mitsuhiro Nogami,[1] Toshiyuki Onodera,[2] and Keitaro Hitomi[1]

[1]Department of Quantum Science and Energy Engineering, Tohoku University, Sendai, Miyagi 980-8579, Japan
[2]Department of Electrical and Electronic Engineering, Tohoku Institute of Technology, Sendai, Miyagi 982-8577, Japan
[3]Thallous Labo. Co., Ltd., Osaki, Miyagi 989-6711, Japan

(Received October 18, 2023; accepted January 5, 2024)

Keywords: TlBr semiconductor detector, plasma etching, X-ray photoelectron spectroscopy (XPS)

The changes in thallium bromide (TlBr) surfaces induced by plasma etching were characterized by X-ray photoelectron spectroscopy (XPS). A TlBr crystal was grown by the traveling molten zone method with zone-purified material. TlBr wafers were obtained from the crystal. Ar plasma etching was performed on the TlBr wafers. XPS revealed that Tl metal (Tl^0) was created in TlBr by the plasma etching. The Tl^0 concentration increased with the irradiation time of the plasma. The net Tl^0 concentrations of TlBr wafers etched by the plasma for 45 and 180 s were 0.7 and 2.6 wt%, respectively.

1. Introduction

Thallium bromide (TlBr) has been studied as a promising material for semiconductor radiation detectors that can operate at room temperature. Three performance indicators for semiconductor radiation detectors are (1) radiation detection efficiency, (2) energy resolution, and (3) stability.

The radiation detection efficiency depends on the type and energy of the incident radiation, and is determined by factors such as the elemental composition, density, and thickness of the sensitive region for the radiation incident direction. For gamma rays, the higher the atomic number Z, the greater the interaction probability; the higher the density of the sensitive volume, the higher the probability of the interaction with the radiation; and the thicker the sensitive region, the greater the absorption probability of incident radiation according to the Beer–Lambert law. However, the detector thickness is limited by factors such as the charge collection efficiency and the size of the single crystal.

The energy resolution is mainly affected by the carrier mobility–lifetime ($\mu\tau$) product and the dark current of the detector. Electron–hole pairs are generated when the incident radiation interacts with the detector material, the number of which is proportional to the energy of the incident radiation and depends on the pair creation energy of the single crystal. Drift current is

*Corresponding author: e-mail: nojima.taro.p1@dc.tohoku.ac.jp
https://doi.org/10.18494/SAM4703

ISSN 0914-4935
https://myukk.org/

induced by these pairs when an electric field exists, and the induced charges are observed as a pulse in an external circuit. When carrier traps exist at a high density in the single crystal, τ decreases, whereas decreases in μ are mainly due to the disorder of the crystallinity of the single crystal or the inclusion of impurities. With decreasing $\mu\tau$, the pulse height decreases depending on the carrier drift length determined by the interaction position of the incident radiation. Thus, the energy resolution of the detector with a low $\mu\tau$ product depends on the position of the gamma-ray interaction. A higher $\mu\tau$ results in a lower signal deficit during the charge carrier drift, giving a higher energy resolution. The dark current, which causes noise in external circuits, flows through the detector regardless of the incident radiation. Thus, it is important to reduce the dark current to obtain high energy resolution. In practical applications, it is desirable that the dark current is not only sufficiently low but also has long-term stability.

The stability of semiconductor radiation detectors depends on factors related to the material of the single crystal and the detector structure. High stability is required for the detector to operate continuously with high energy resolution.

In terms of radiation detection efficiency, TlBr has been reported to be one of the best semiconductor detector materials, because it contains thallium (atomic number: 81) and has a high density of 7.56 g/cm^3. The energy resolution of TlBr detectors has been increased by increasing $\mu\tau$ and improving the electrode structure, and a value of approximately 1% (662 keV) has been recently reported.[1] Regarding the dark current, which is a factor affecting the energy resolution, there is a large difference between its reported values, with the dark current depending on the electrode material.[2,3] TlBr detectors with noble metal electrodes suffer from the phenomenon of polarization, which causes a decrease in the pulse height obtained from the detector and electrode deterioration during long-term operation. To address this problem, measures such as low-temperature operation,[4] bias switching,[5] and the use of Tl electrodes in the detector[6] have been proposed, with the use of Tl electrodes being the most effective approach. However, there are problems with Tl electrodes, such as large differences in dark current among detectors and poor fabrication yield. Some TlBr detectors with Tl electrodes exhibit an increased dark current upon applying bias voltage shortly after fabrication, resulting in the failure of the detector operation. We speculate that the differences in dark current among detectors and the poor fabrication yield are probably due to the same causes, such as the structure and condition of the electrode–crystal interface. Furthermore, TlBr is an ionic conductor,[7] and the large differences in dark current among detectors can be caused by the complex behavior of ionic conduction and electrode reactions in the detector. Because these electrode reactions are considered to be strongly affected by surface conditions, chemical etching[8] and plasma etching have been proposed as surface treatment methods. Although surface treatment with plasma etching has been reported to improve detector performance,[9,10] it is not well understood how the surface conditions change. In this study, the effect of plasma etching on a TlBr surface was investigated to reveal how the state of the electrode interface affects the detector behavior.

2. Data, Materials, and Methods

2.1 Materials

A detector-grade TlBr single crystal was used as the sample for surface measurements. The starting material was anhydrous beads (Merck & Co., Inc.) with 5N (99.999%) purity, purified by zone melting (364 passes). The single crystal was grown by the traveling molten zone technique in a HBr atmosphere, then sliced into wafers using a diamond wire saw. The TlBr wafers were polished with P2000 (8 mm) SiC abrasive paper on both sides to a thickness of approximately 2 mm, then ultrasonically cleaned in ethanol.

2.2 Plasma treatment

Plasma etching was performed using a tabletop plasma etching device (model TP-50B, Sanyu Co., Ltd.). In this study, pure Ar was used as the process gas. The process was performed under an Ar pressure of 1000 Pa with a gas flow of 50 sccm and an RF power of 10 W. Three TlBr wafers were prepared in this study: a wafer without plasma treatment (S0) and wafers etched by plasma for 45 s (S1) and 180 s (S2). The 45 s plasma treatment yielded TlBr detectors with good performance in our laboratory. To reveal the effect of long treatment time, the plasma treatment time four times longer (180 s) was chosen. Although the wafers were in an inert atmosphere during the plasma treatment, the system required at least 15 min to vent the specimen chamber. The wafers were placed in a vacuum desiccator immediately after being exposed to the atmosphere. The wafers were stored at 0.05 atm or less for about 2 weeks before being placed in the high-vacuum chamber of an X-ray photoelectron spectroscopy (XPS) system.

2.3 XPS measurement

To characterize the chemical surface condition of TlBr, XPS measurements were performed on the three TlBr wafers (S0, S1, and S2) using an XPS system (AXIS-ULTRA, Shimadzu Corporation) with a monochromatic Al Kα source (1486.7 eV). The X-ray beam was elliptical (0.3 × 0.7 μm) and the detector was located normal to the sample. XPS spectra were acquired with a pass energy of 20 eV (narrow scan) or 160 eV (wide scan) with a resolution of 0.45 eV. During the XPS measurements, the TlBr samples became charged owing to the high resistivity of the crystals. To avoid peak shifts for photoelectrons caused by charging, neutralization was performed using an electron flood gun. XPS depth profile analyses with Ar etching were performed for the TlBr samples. In Ar etching, the acceleration voltage was 4.86 V, the current was 5 mA, and the raster range was 2 × 2 mm^2. Ar etching was performed five times for each sample, and the XPS spectrum was measured after each etching. The duration of each etching was 1 min, corresponding to an Ar etching rate of 2.5 nm/min in SiO_2. The obtained XPS spectra were analyzed using CasaXPS software to calculate the surface composition. The binding energy is commonly calibrated using the C 1*s* peak of adventitious carbon.[11] However, the main peak of Tl for TlBr (119.20 eV[12]) was employed for the energy calibration because of the low intensity of the C 1*s* peak after Ar etching in this study. The Tl *4f*, Br *3d*, O *1s*, and C *1s* core-level peaks were fitted using the Shirley background and Gaussian–Lorentzian line shapes.

3. Results

Figure 1 shows images of TlBr wafers under a metal mask without (S0) and with (S1) the plasma etching treatment. As can be seen in the figure, the TlBr wafer became darker during the plasma treatment or venting.

No peaks other than Tl, Br, O, and C were detected in the wide-scan XPS measurements, indicating that the concentration of other elements was less than 1 atm%, reflecting the high purity of the crystal. Tl 4*f* core-level peaks at the outermost surfaces of S0, S1, and S2 are shown in Fig. 2 and their depth profiles are shown in Fig. 3. The Br *3d*, O *1s*, and C *1s* core-level peaks at the outermost surfaces of the samples are shown in Fig. 4. The XPS spectrum for Tl *4f* exhibited a doublet division. The average measured energy difference between the peaks was 4.44 eV. A subpeak on the low-energy side of the main Tl *4f* peak was observed with an average energy of 117.47 eV for the outermost surfaces of S1 and S2 (blue line in Fig. 2) and on all samples after Ar etching. It is known that Ar etching changes metal oxides to lower-valence or metal states.[12] Considering that this phenomenon also occurred in TlBr in this study, we inferred that metal Tl (Tl^0) was generated by Ar etching since Tl in TlBr is monovalent. In the combination of elements detected after Ar etching, the possible chemical states of Tl are Tl^0, Tl_2O, Tl_2O_3, and TlBr, corresponding to energies of 117.1, 119.1, 118.6, and 119.2 eV, respectively.[13] Since the energy of Tl^0 is close to the measured energy of the subpeak, it was concluded that the subpeak represents Tl^0. The main Tl *4f* peak was considered to be mainly TlBr; thus, we expressed it as Tl (TlBr). When we calculated the surface composition, the Tl (TlBr) peak and the Tl (Tl^0) subpeak were quantified separately. The binding energy of the Br *3d* peak was 69.47 eV, which was consistent across all samples and depths, indicating that the chemical bonding state of Br is single (TlBr). The C *1s* peak was prominent on the outermost surface. Because a rapid decrease in C *1s* peak intensity was observed after Ar etching, the origin of the peak was concluded to be adventitious carbon. The O *1s* spectrum had a broad peak in the range of 530–535 eV, suggesting the presence of components with different chemical bonding states. We considered that a certain amount of oxygen derived from the adventitious carbon was on the outermost surface. Because the concentration of C 1*s* became low after Ar etching and TlBr was highly pure, we considered that oxygen paired with Tl (to form, for example, Tl_2O). The quantitative results of the XPS measurements are summarized in Tables 1–3.

4. Discussion

In Tables 1–3, the ratio of Tl (TlBr) to Br is greater than one for all data, whereas it should be one for TlBr. This discrepancy was mainly due to the presence of Tl oxides and/or etching products in the samples. Because the binding energy of Tl_2O is 119.1 eV, which is inseparable from that of TlBr (119.2 eV), the quantitative results for Tl (TlBr) probably contained a contribution originating from Tl_2O. No peak corresponding to Tl_2O_3 was detected in the samples. A probable etching product that increased the Tl (TlBr)/Br ratio was Br_2, which easily evaporated from the sample, as described later.

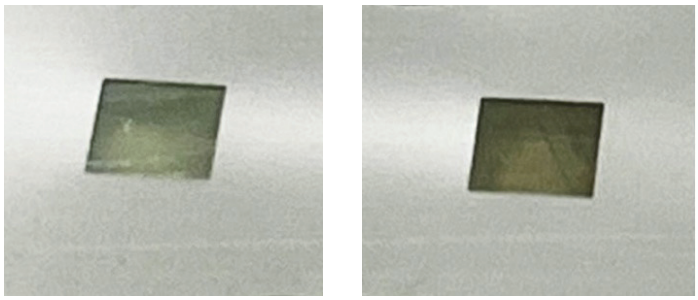

(a) (b)

Fig. 1. (Color online) TlBr samples covered with a metal mask: (a) without plasma treatment and (b) with 45 s plasma treatment.

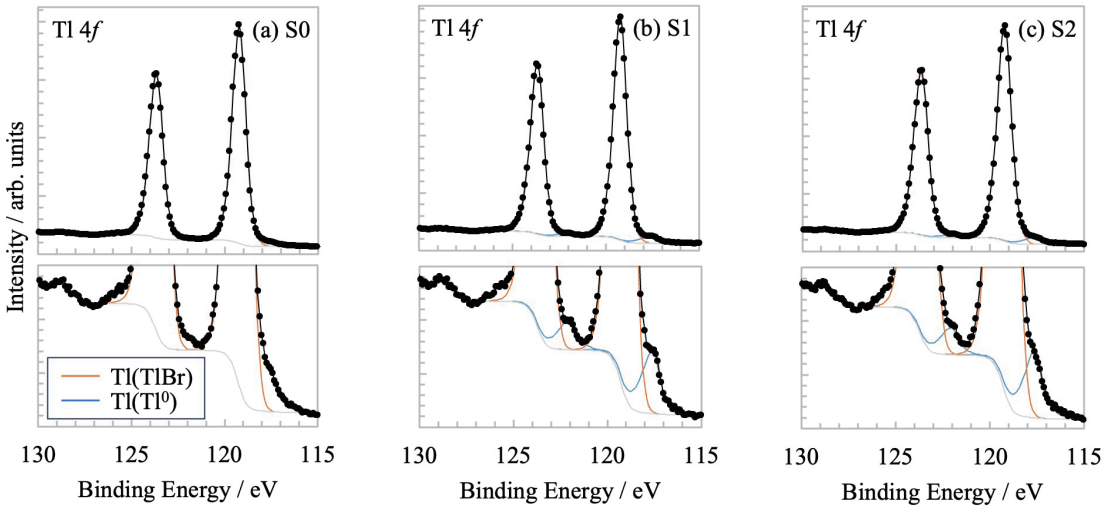

Fig. 2. (Color online) Tl 4*f* core-level peaks at the outermost surfaces of (a) S0, (b) S1, and (c) S2.

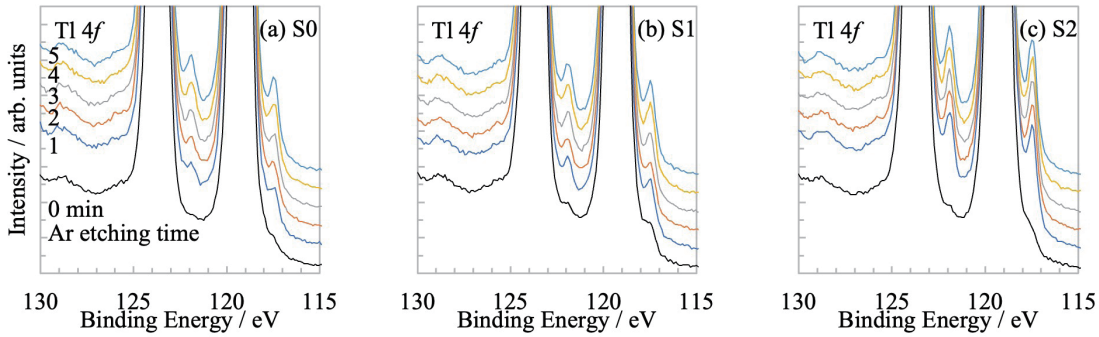

Fig. 3. (Color online) Depth profiles of Tl 4*f* core-level peaks for (a) S0, (b) S1, and (c) S2.

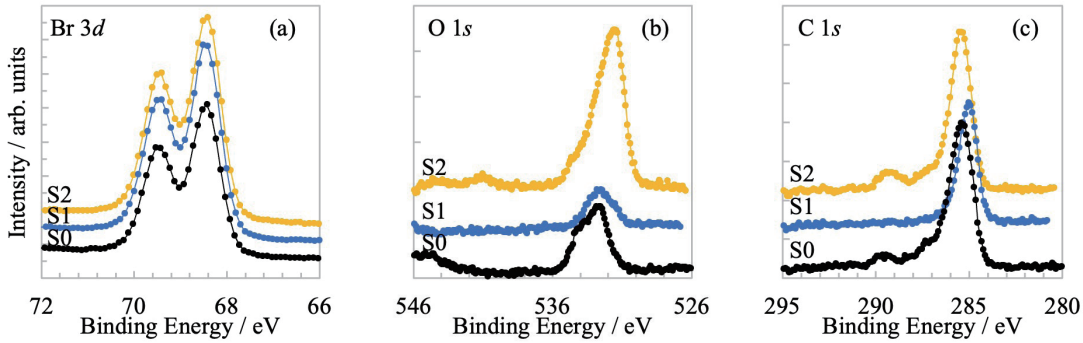

Fig. 4. (Color online) (a) Br 3*d*, (b) O 1*s*, and (c) C 1*s* core-level peaks at outermost surfaces of S0, S1, and S2.

Table 1
XPS quantitative results for S0 (atm%, no plasma etching treatment).

Etching time (min)	0	1	2	3	4	5
Tl (TlBr)	26.7	51.6	51.9	51.9	51.7	52.2
Br	23.1	45.3	45.2	45.8	45.5	45.7
Tl (Tl^0)	N.D.	1.7	1.9	1.8	2.3	2.1
O	6.9	1.4	1.1	0.5	0.5	N.D.
C	43.3	–	–	–	–	–

Table 2
XPS quantitative results for S1 (atm%, plasma etching treatment for 45 s).

Etching time (min)	0	1	2	3	4	5
Tl (TlBr)	34.1	51.1	51.3	51.6	51.5	51.6
Br	30.1	44.2	44.3	44.6	44.7	44.8
Tl (Tl^0)	1.4	2.0	2.3	2.4	2.6	2.7
O	4.4	2.6	2.0	1.4	1.2	0.9
C	30.0	–	–	–	–	–

Table 3
XPS quantitative results for S2 (atm%, plasma etching treatment for 180 s).

Etching time (min)	0	1	2	3	4	5
Tl (TlBr)	25.7	47.6	48.2	49.1	49.9	50.2
Br	18.2	36.6	39.2	40.4	41.3	42.1
Tl (Tl^0)	1.0	3.8	3.7	3.7	3.8	3.9
O	16.3	12.0	8.9	6.8	5.0	3.9
C	39.1	–	–	–	–	–

The Ar etching time dependence of the Tl (Tl^0) concentration in the samples is shown in Fig. 5(a). The Tl (Tl^0) concentration was normalized with the Br concentration, which is expected to represent the TlBr concentration in the samples. The error bars represent the standard deviations of the XPS measurements, which were assumed to be 0.2 atm%. With increasing plasma treatment time, the Tl (Tl^0)/Br ratio tends to increase for all samples. Tl (Tl^0) mainly originated from the plasma treatment and Ar etching before and during the XPS

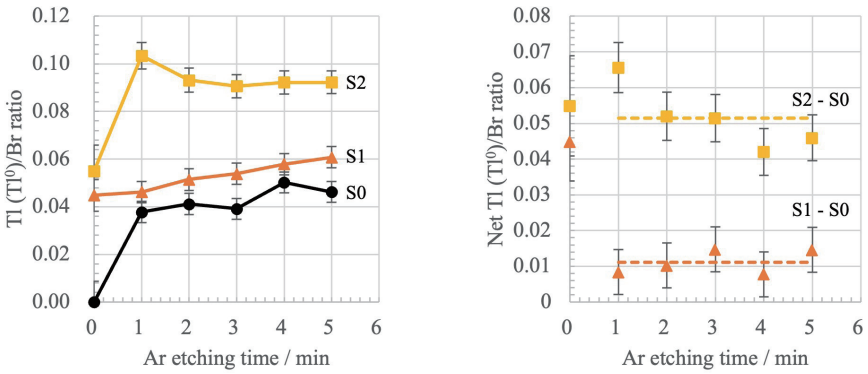

(a) (b)

Fig. 5. (Color online) Ar etching time dependences of (a) Tl(Tl0)/Br ratio and (b) net Tl(Tl0)/Br ratio.

measurements, respectively. Because no Tl (Tl^0) (or an amount less than the detection limit) was observed for the outermost surface of S0, the Tl (Tl^0)/Br ratio for S0 (with no plasma treatment) should reflect the concentration of Tl^0 generated only by Ar etching. Since the Ar etching conditions were constant, Tl^0 should have been generated at a constant rate for all samples. The net Tl (Tl^0)/Br ratio for plasma treatment was calculated by subtracting the value for S0 from the values for S1 and S2 [Fig. 5(b)]. The net Tl (Tl^0)/Br ratio tended to become constant after Ar etching for 1 min. The average values for S1 and S2 were 0.01 and 0.05, corresponding to 0.7 and 2.6 wt% of Tl^0, respectively. The wt% values were estimated with the oxygen concentrations in the samples ignored. S1 and S2 were subjected to plasma treatment under the same conditions, with the only difference being that the irradiation time was four times longer for S2 than for S1. The net Tl (Tl^0)/Br ratio of S2 was about five times that of S1, which implies that the Tl^0 concentration was correlated to the irradiation time. In other words, the plasma treatment generated Tl^0 at a constant rate and its depth distribution was uniform to a depth of at least 12.5 nm (SiO_2 equivalent). Note that XPS gives the average concentration within the measurement region, and other approaches are required to obtain the in-plane distribution of Tl^0.

The results of the XPS measurements imply that Tl^0 is involved in the discoloration caused by the plasma treatment shown in Fig. 1. This discoloration is assumed to be due to the generated Tl^0 itself or to Tl_2O formed by the oxidation of the outermost Tl^0 exposed to the atmosphere. In the case of silver halide, Ag^0 is produced by photolysis upon irradiation with UV light in vacuum.[14,15] The formation of Tl^0 in TlBr by the Ar plasma treatment can be explained by analogy with the photolysis of silver halide. During the Ar plasma treatment of the TlBr sample, electron–hole pairs are created on the crystal surface by the irradiation of Ar ions and UV light from the plasma. The holes created by the Ar plasma may oxidize Tl^+ and Br^- to Tl^{3+} and Br (resulting in Br_2), respectively. The halogen molecular gas has a high vapor pressure and is easily gasified from the surface. Since the plasma processing conditions were a low vacuum with a gas flow in this study, the generated Br_2 gas on the surface will easily evaporate. The electrons created by the Ar plasma may reduce Tl^+ and Tl^{3+} to Tl^0 and Tl^+, respectively. The creation of Tl^0 on the TlBr surface by Ar plasma treatment is expected to improve the performance of TlBr detectors.

5. Conclusions

The effect of plasma etching as a surface treatment for TlBr detectors was investigated by XPS. Tl^0 was observed on the outermost surface of TlBr etched by Ar plasma and on all samples after Ar etching during XPS measurements. The formation of Tl^0 can be explained by analogy with the photolysis of silver halide. The net Tl^0 concentrations of TlBr wafers etched by the plasma for 45 and 180 s were 0.7 and 2.6 wt%, respectively. The formation of Tl^0 by plasma etching is expected to improve the performance of TlBr detectors. Future investigation will be directed toward revealing the role of Tl^0 between the electrode and the crystal in affecting the behavior of the TlBr detectors.

Acknowledgments

This work was supported by JSPS KAKENHI Grant Number JP20H00656.

References

1 C. Leak, W. Koehler, S. O'Neal, Z. He, and K. Hitomi: 2016 IEEE Nuclear Science Symposium, Medical Imaging Conference and Room-Temperature Semiconductor Detector Workshop (NSS/MIC/RTSD) (2016) 1–3. https://doi.org/10.1109/NSSMIC.2016.8069952
2 A. Datta and S. Motakef: IEEE Trans. Nucl. Sci. **62** (2015) 437. https://doi.org/10.1109/TNS.2015.2400396
3 V. Gostilo, A. Owens, M. Bavdaz, I. Lisjutin, A. Peacock, H. Sipila, and S. Zatoloka: IEEE Trans. Nucl. Sci. **49** (2002) 2513. https://doi.org/10.1109/TNS.2002.803858
4 H. Kim, A. Kargar, L. Cirignano, A. Churilov, G. Ciampi, W. Higgins, F. Olschner, and K. Shah: IEEE Trans. Nucl. Sci. **59** (2012) 243. http://doi.org/10.1109/TNS.2011.2173503
5 A. Datta, J. Fiala, P. Becla, and S. Motakef: APL Mater. **5** (2017). https://doi.org/10.1063/1.5001181
6 K. Hitomi, T. Shoji, and Y. Niizeki: Nucl. Instrum. Methods Phys. Res., Sect. A **585** (2008) 102. https://doi.org/10.1016/j.nima.2007.11.012
7 S. R. Bishop, W. Higgins, A. Churilov, G. Ciampi, H. Kim, L. Cirignano, V. Biteman, J. Tower, K. Shah, and H. Tuller: ECS Trans. **28** (2010) 333. https://doi.org/10.1149/1.3495857
8 L. F. Voss, A. M. Conway, R. T. Graff, P. R. Beck, R. J. Nikolic, A. J. Nelson, S. A. Payne, H. Kim, L. Cirignano, and K. Shah: IEEE Nuclear Science Symposuim & Medical Imaging Conf. (2010) 3746–3748. https://doi.org/10.1109/NSSMIC.2010.5874511
9 S. Motakef and A. Datta: 2015 IEEE Nuclear Science Symposium and Medical Imaging Conf. (NSS/MIC) (2015) 1–2. https://doi.org/10.1109/NSSMIC.2015.7582281
10 A. Datta, P. Becla, and S. Motakef: Sci. Rep. **9** (2019) 9933. https://doi.org/10.1038/s41598-019-46360-z
11 M. C. Biesinger: Appl. Surf. Sci. **597** (2022) https://doi.org/10.1016/j.apsusc.2022.153681
12 S. Hashimoto, K. Hirokawa, Y. Fukuda, K. Suzuki, T. Suzuki, N. Usuki, N. Gennai, S. Yoshida, M. Koda, H. Sezaki, H. Horie, A. Tanaka, and T. Ohtsubo: Surf. Interface Anal. **18** (1992) 799. https://doi.org/10.1002/sia.740181204
13 A. J. Nelson, J.-S. Lee, J. A. Stanford, W. K. Grant, L. F. Voss, P. R. Beck, R. T. Graff, E. L. Swanberg, A. M. Conway, R. J. Nikolic, S. A. Payne, H. Kim, L. J Cirignano, and K. Shah: Proceedings Volume 8852, Hard X-Ray, Gamma-Ray, and Neutron Detector Physics XV (2013). https://doi.org/10.1117/12.2021675
14 G. W. Luckey: J. Phys. Chem. **57** (1953) 791. https://doi.org/10.1021/j150509a012
15 G. W. Luckey: J. Chem. Phys. **23** (1955) 882. https://doi.org/10.1063/1.1742141